Temporal Pulse Shaping of Fiber-Optic Laser Beams

S. C. Burkhart

F. A. Penko

Introduction

Precise temporal pulse-shaping of the laser beams for inertial confinement fusion (ICF) experiments has become increasingly important over the last 15 years, as better understanding has been made of optimal target drive conditions.[1] ICF targets have been shown to reach higher temperatures and better convergence when the laser drive is increased in a controlled manner during the drive pulse duration, which mitigates premature heating of the capsule interior. Computer simulations and experimental campaigns have confirmed the advantages of such a shaped laser drive. Another consideration is that small asymmetries in the initial laser drive imprint on the capsule, preventing implosion symmetry and limiting capsule convergence. This puts high value upon balancing the power for the multiple beams of lasers like Nova, Omega, or the National Ignition Facility (NIF). Since each beamline behaves somewhat differently, temporal shaping capability for each beam is planned for the NIF to achieve power balance. Finally, temporal pulse shaping is required to correct for pulse distortion due to gain saturation in the main amplifiers, which can cause the end of an initially square temporal pulse to droop by factors of up to 15:1 at the laser output. To achieve independent pulse shaping on the NIF, an integrated electrooptic modulator driven by a ~ 5-V arbitrary pulse shape generator will be used for the front end of the laser system,[2] when each laser beam is at low energy ($< 1\ \mu J$), as shown in Fig. 1. This article discusses the design and performance of this device.

Background

To date the Nova, Omega, Phebus, and Shiva lasers have all used conventional optical oscillators and amplifiers for laser-pulse generation, requiring bulk KDP Pockels cells for temporal pulse shaping.[3] Depending on the design, these Pockels cells have a half-wave voltage of either 4 or 8 kV, which places severe demands on the electrical waveform generation due to the high voltages. For Nova, the shaped pulse is derived from a square high-voltage pulse, generated by a photoconductive silicon switch[4] that discharges an initially charged 25-Ω transmission line. The square pulse is injected into a section of nonuniform transmission line designed to reflect an electrical pulse shape, generating the desired optical pulse shape through the Pockels cell. On Nova, the transmission line initially consisted of a microstrip line, but this was soon replaced by a variable impedance transmission line (VITL),[5] a manually adjustable nonuniform line. In 1989, Nova abandoned the VITL and returned to the microstrip transmission lines due to the difficulty in retuning the VITL to previously generated pulse shapes. Also in 1989, a numerical method for calculating the required stripline impedance was developed,[6] a

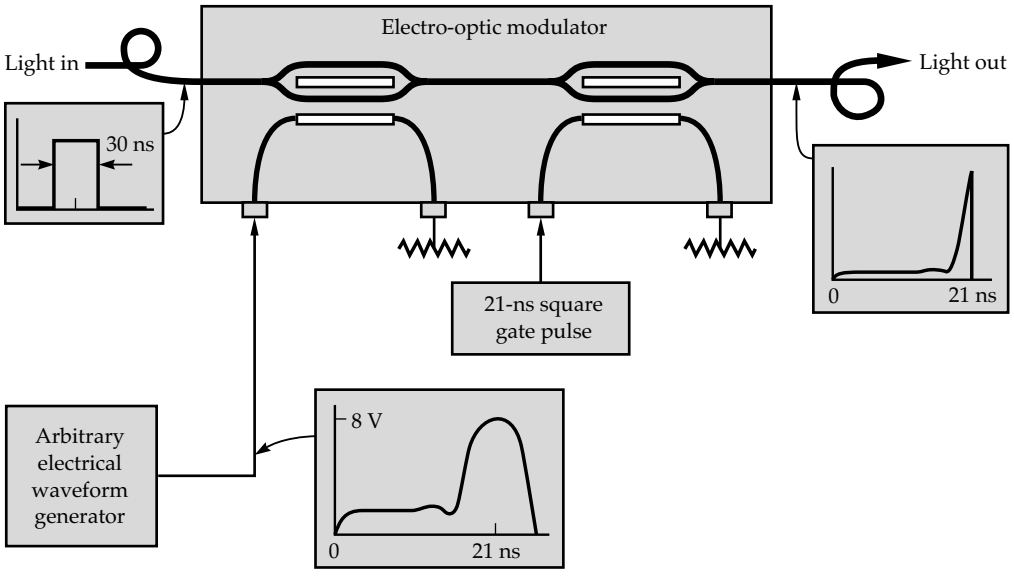

FIGURE 1. The NIF pulse-shaping system, comprised of an electrooptic modulator, a square pulse generator, and an arbitrary electrical waveform generator. The electrooptic modulator (two Mach–Zehnder interferometers) modulates the fiber-provided laser light using electrical pulses from the arbitrary waveform generator (AWG) and the square pulse generator. The second Mach–Zehnder interferometer is necessary to achieve > 10^5 on/off contrast. (70-50-0195-0185pb01)

technique now implemented on Omega and Phebus. The limitation of this technique is that each different pulse shape requires a new microstrip transmission line to be fabricated, similar to that shown in Fig. 2.

One major development from the Beamlet project[7] is a new type of laser master oscillator and pulse shaping system based on 1.053-μm fiber-optic lasers and components.[8] In this new system, beam intensity is controlled by an integrated optic Mach–Zehnder interferometer (electrooptic modulator), which has an extinction voltage of only 10 V. This advance opened up new approaches to pulse shaping, which on Beamlet was originally accomplished using transmission lines periodically coupled by potentiometers. This arrangement provided pulse-adjustment capability for monotonically increasing pulses, but was still was not amenable to computer control.

In 1994, we began to develop a fully computer-controllable electrical pulse shaping system capable of driving the Beamlet-style electrooptic modulator. Haner and Warren[9,10] set precedence for this approach by developing an electrical technique based on microwave GaAs field-effect transistors (FETs) to generate subnanosecond shaped pulses for laser beam modulation and subsequent compression to subpicosecond duration. Their circuit consisted of six GaAs-FETs connected in parallel through coupling capacitors to construct short shaped pulses. The method of Haner and Warren demonstrated the speed needed for ICF lasers, but the parallel connection approach was not extendable to large numbers of GaAs-FET sections. The arbitrary waveform generator (AWG) we developed bypassed these limitations by using a traveling wave architecture and a reflection-free trigger system. We have modeled[11] the circuit, performed device characterization experiments, and fabricated a 14-element unit.

Waveform Generator Principles

The waveform generator is based on the summation of short (250-ns) pulses sequenced in time and with differing amplitudes. This is similar to the digital-to-analog converter in a compact disc player, but at a speed beyond the state of the art. In the following two sections, we describe the wave-summing approach and discuss some of the practical issues with the electrical circuitry.

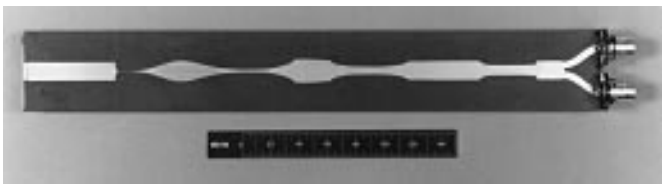

FIGURE 2. An example of the nonuniform transmission lines synthesized for pulse shaping on the Nova laser. This particular nonuniform transmission line generates a "picket-fence" pulse, consisting of two small prepulses followed by a main drive pulse, for Nova target experiments. (70-50-0396-0503pb01)

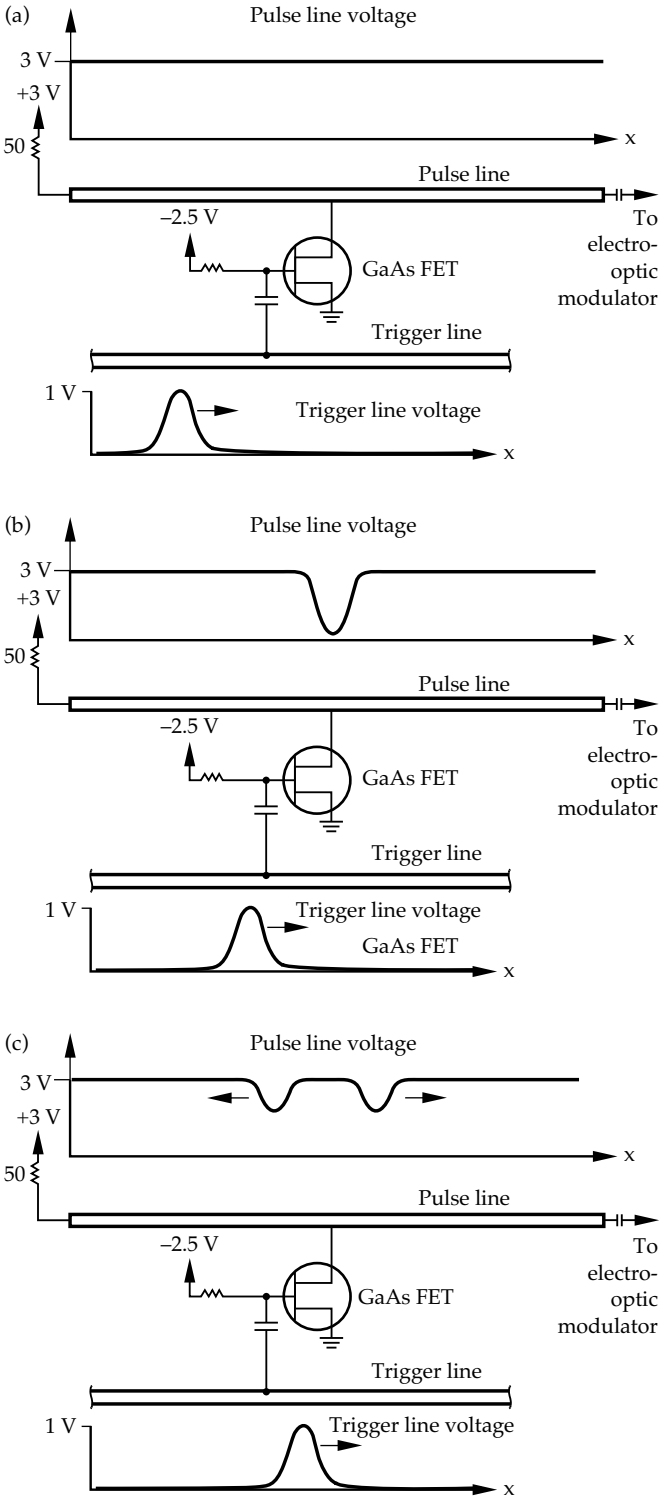

FIGURE 3. The AWG concept in three stages: (a) A 1-V trigger pulse is launched onto the trigger transmission line. The initially quiescent pulse transmission line is tied to +3 V through a termination resistor. (b) The trigger pulse turns on the GaAs field-effect transistor (FET) as it propagates past the coupling capacitor. This creates a dip in the pulse line voltage proportional to the initial GaAs-FET bias voltage (–2.5 V). (c) The voltage dip is really composed of two counterpropagating pulses: the pulse traveling to the right becomes part of the shaped pulse, and the pulse propagating to the left is absorbed by the termination. The trigger pulse propagates to the next GaAs-FET stage. (70-50-0396-0504pb01)

Impulse Generation and Traveling Wave Summation

Arbitrary waveforms are assembled using a large number of the basic circuit sections shown in Fig. 3. Each section consists of a power GaAs-FET connected between the charged transmission line and ground, activated by the impulse from the trigger line. When 1 V of the trigger impulse is coupled to the GaAs-FET gate, it turns on, conducting current in proportion to the initial bias pulse on the gate, as shown in Fig. 3(b). An opposite polarity replica of the trigger pulse is generated onto the pulse line, composed of two counterpropagating pulses each containing half the amplitude. The left-going pulse is absorbed by a terminator shown on the left side of Fig. 3, but the right-going pulse becomes part of the overall shaped pulse. The amplitude of the generated pulse is dependent upon the initial bias (V_{b1}, V_{b2}, etc.), because the GaAs-FET does not turn on until the gate voltage exceeds approximately –2.2 V relative to the source (the grounded terminal in this circuit). If the bias is initially set to –4.0 V, the 1-V trigger pulse does not turn on the GaAs-FET and no impulse is generated on the pulse line. On the other hand, if the bias is initially –2.2 V, it turns on strongly, making an impulse in excess of 1 V. For bias voltages intermediate between these two extremes, the impulse amplitude follows a square law, $I_{ds} \propto (V_{gs} - V_{TO})^2$ where V_{gs} is the gate-to-source voltage due to the bias plus the trigger voltages and V_{TO} is the gate cutoff voltage (nominally –2.2 V).

Each of the elemental impulses traveling to the right becomes a time-slice of the overall shaped pulse (Fig. 4). The timing between the trigger line and the pulse line is set to generate impulses at a specific rate. We chose four gigasamples per second (GS/s) based on an analysis of the temporal resolution required to synthesize NIF pulse shapes. For this data rate, the trigger delays shown in Fig. 4

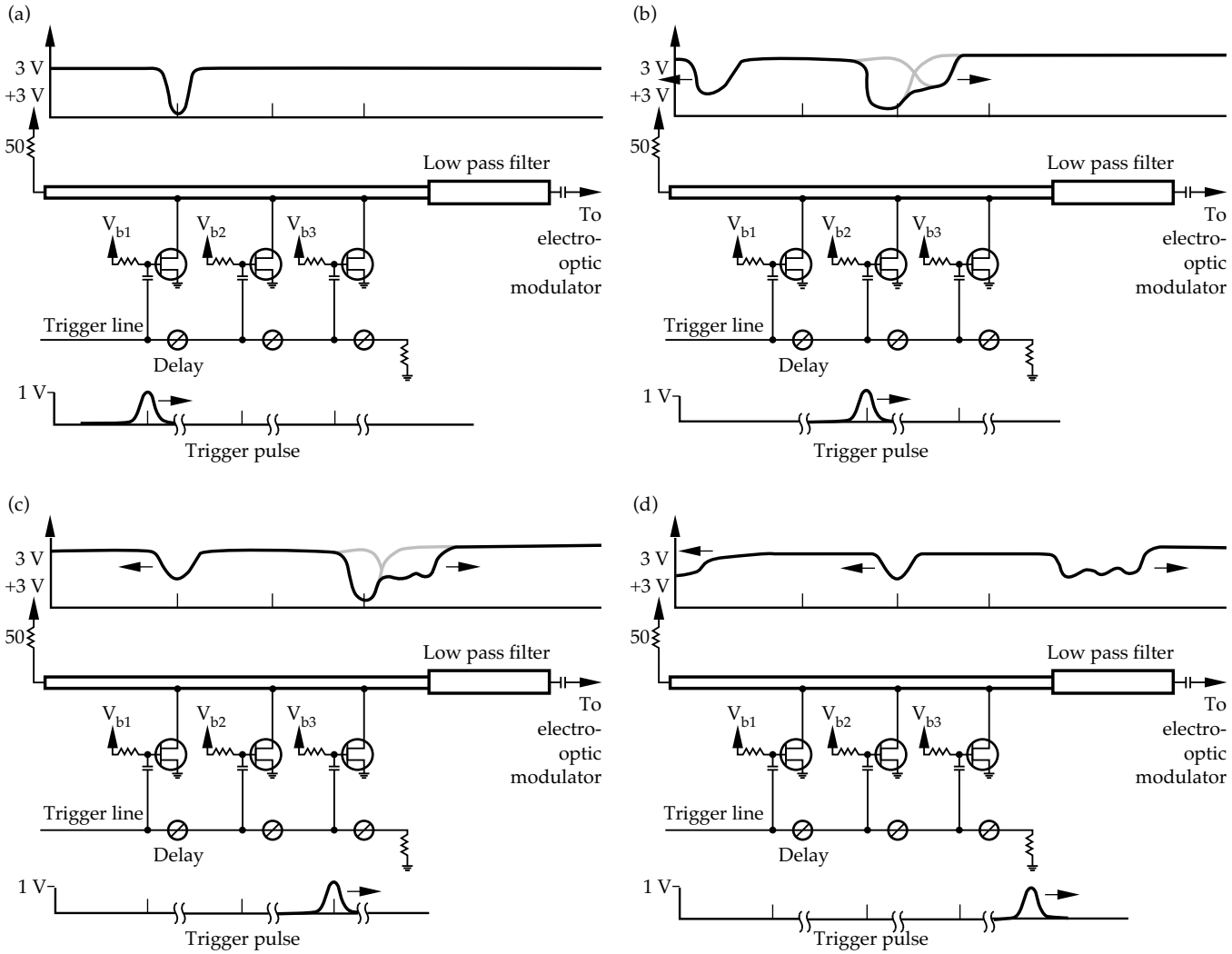

FIGURE 4. A square pulse generated from three pulses. (a) The first pulse is generated by the first GaAs-FET, with the pulse amplitude set by the bias voltage V_{b1}. For this drawing, $V_{b1} = V_{b2} = V_{b3}$. (b) The trigger pulse delay makes the second GaAs-FET turn on just after the first pulse propagates past, summing the second impulse (set by V_{b2}) to the shaped pulse. (c) A third impulse (set by V_{b3}) is added onto the end of the shaped pulse. (d) The final, shaped, square pulse remains after the left-propagating pulses have traveled towards the termination. The 4-GHz sinusoid on the top of the square pulse is strongly suppressed by the 1-GHz low-pass filter (not shown). (70-50-0396-0505pb01)

are set to 250 ps plus the FET-to-FET delay along the pulse line. Also, the trigger pulse full width at half maximum (FWHM) is set to between 250 and 350 ps to overlap each subsequent elemental pulse onto the tail end of the previous one. The elemental pulses are summed with each amplitude independently set by the computer-controlled gate-bias voltages. The harmonics at multiples of the sampling frequency (4 GHz for our design) are suppressed by a 1.0-GHz maximally linear phase (Bessel) low-pass filter at the generator output. This constitutes a 4-GS/s AWG, with a 1-GHz bandwidth, and a pulse length limited only by the number of GaAs-FETs sequenced along the transmission line. Presently, commercial waveform generators are limited to 1 GS/s, with a bandwidth of 200 Mhz, at a cost unacceptable to the NIF Project.

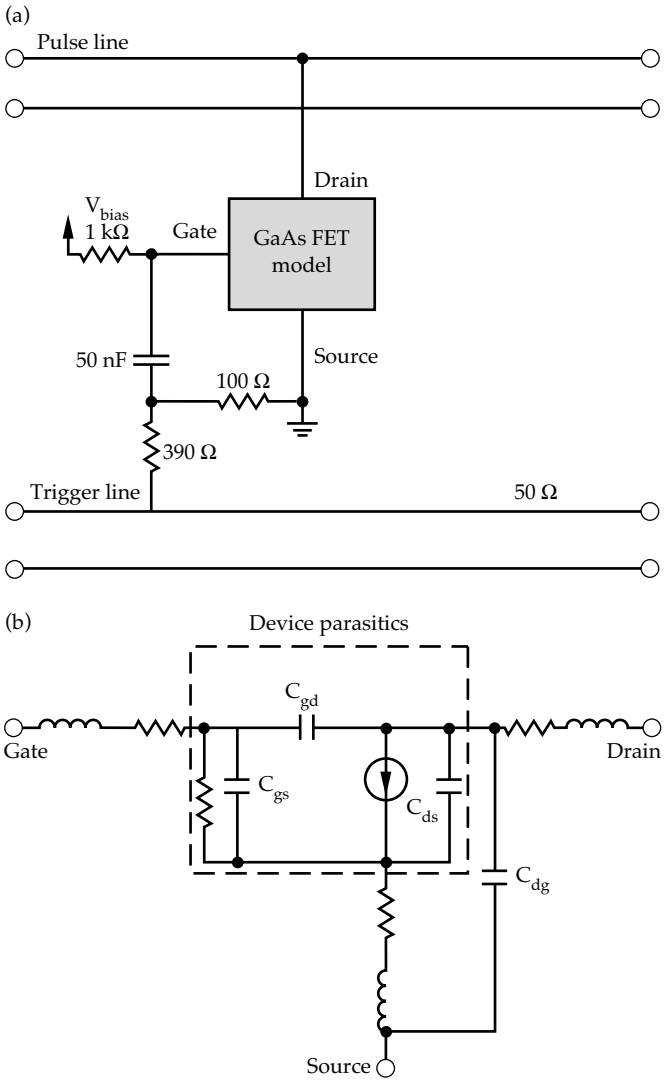

FIGURE 5. Circuit representation of each GaAs-FET section. (a) Bias is provided through a 1-kΩ resistor, and the trigger pulse propagates through the 50-nF capacitor to the GaAs-FET gate. The 100-Ω resistor to ground speeds up the switching. (b) Detailed model of the GaAs-FET parasitic elements. The key elements are C_{gd} and C_{ds}, which cause discontinuities (and reflections) on the pulse line. We compensate for the capacitive load by decreasing the line impedance. (70-50-0396-0506pb01)

Transmission Line Compensation and Trigger Distribution

Figure 5 shows the complete circuit model for the "building block" described above. Ideally, the GaAs-FET acts as a voltage-controlled current source when on and as an open circuit when off. This ideal behavior is modified by the stray inductance, capacitance, and lead resistance inherent in the GaAs-FET structure and the packaging, as shown in Fig. 5(b). Circuit modeling and experiments demonstrated that 4-GS/s operation is possible if the gate node impedance is less than 240 Ω. Going to higher speeds (more than 4 GS/s) requires a lower gate impedance with a commensurate increase in trigger-pulse attenuation.

The other significant parasitics are C_{gd} and C_{ds}. [Fig. 5(b)]. These capacitances effectively load the pulse line with distributed capacitance, lowering the transmission line impedance. This is shown by the measured time domain reflectometer (TDR) trace looking into a 14-element AWG in Fig. 6. The unloaded line impedance of 56 Ω decreased to 38.5 Ω when loaded with the GaAs-FETs. We found that we could compensate for GaAs-FET loading by increasing the line impedance such that it became 50 Ω when loaded. This requires precise knowledge of the parasitics, which we obtained by de-embedding[12] them using the manufacturer's S-parameters. We applied the de-embedding technique to the Mitsubishi MGF1801B GaAs-FET and obtained an equivalent shunt capacitance of 0.63 pF. This compares quite well to 0.56 pF calculated from the TDR data in Fig. 6.

Trigger pulse distribution is another important consideration for a long series of GaAs-FET sections. The trigger pulse is attenuated as it triggers each GaAs-FET in sequence, so we developed a technique for maintaining its amplitude. We accomplished this by matching the parallel combination of tap resistor and output trigger line to the input trigger line. This minimized reflective losses and

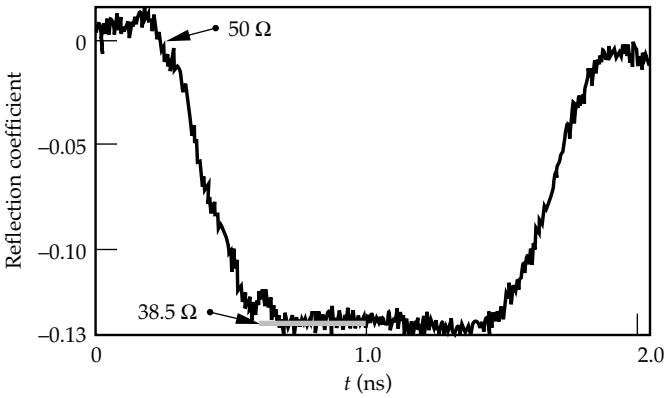

FIGURE 6. Time domain reflectometer (TDR) trace from a 14–GaAs-FET pulse-shaping transmission line. The capacitive loading of the GaAs-FETs reduces the line impedance from 55 to 38.5 Ω. Increasing the line impedance to approximately 80 Ω unloaded results in near 50-Ω performance after the FETs are installed. (70-50-0396-0508pb01)

maintained trigger amplitude within 5% along the 14-section distribution line. We found that it was always advantageous to start the line at the lowest realizable impedance, despite the discontinuity loss where the 50-Ω input cable connected to the printed circuit board. We used 25 Ω as a starting impedance in our prototype because a lower impedance would require an excessively wide transmission line.

Circuit Realization

A 14-stage arbitrary waveform generator was designed and fabricated using the printed circuit shown in Fig. 7.

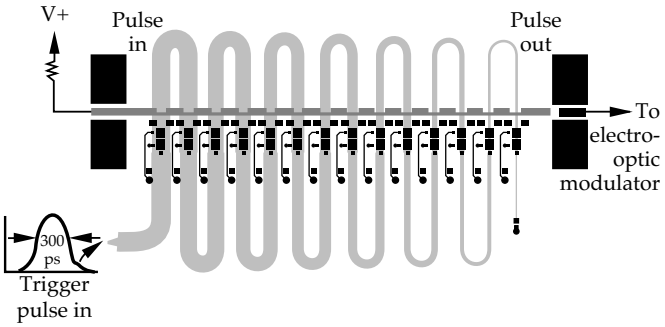

FIGURE 7. Circuit realization of a 14-section AWG. The pulse line is initially charged to voltage (V+), and a 300-ps FWHM trigger pulse is injected into the 25-Ω trigger line. Each GaAs-FET is mounted with its associated circuitry where the pulse lines and trigger lines cross. The printed circuit is constructed from teflon/glass precision microwave circuit board. (70-00-0895-1895pb02)

The circuit board material is a teflon/fiberglass matrix substrate, manufactured to tight tolerances for dielectric constant and substrate thickness, commonly used in microwave circuitry. It is designed as a four-layer board, three layers of 31-mil substrate sandwiched between four layers of copper plating. The first and third layers (starting from the bottom) are ground planes stitched together by numerous plated via holes. The second layer contains the trigger line, which involves a total of 3.5 ns of delay, and the top layer is printed with the pulse line circuit along with mounting pads for all the surface mount components. We used stripline construction for the trigger line to avoid modal dispersion inherent in microstrip, which tends to distort fast pulses. To reduce stray capacitance in the printed circuit, we soldered the GaAs-FETs directly to the edge of the pulse line with a minimum of lead length. Small sections of transistor leads on the board can have large fractions of a picoFarad of stray capacitance, enough to markedly affect the pulse line impedance. The transmission line was manufactured to have a loaded line impedance of $50 \pm 4\ \Omega$. A 4-Ω impedance mismatch causes ~ 4% voltage reflection. In comparison, the highest quality microwave SMA connectors are specified to $50 \pm 2.5\ \Omega$. We also measured the trigger line performance and verified that the trigger pulse maintains its shape and amplitude as it propagates past the 14 GaAs-FETs. There were reflections due to the capacitance of each GaAs-FET gate, but the circuit design mitigated the effect of these reflections.

We built a 28-stage, 7-ns pulse shape generator, consisting of two of the 14-stage circuits, and installed it in the Beamlet laser system. Figure 8 shows the system.

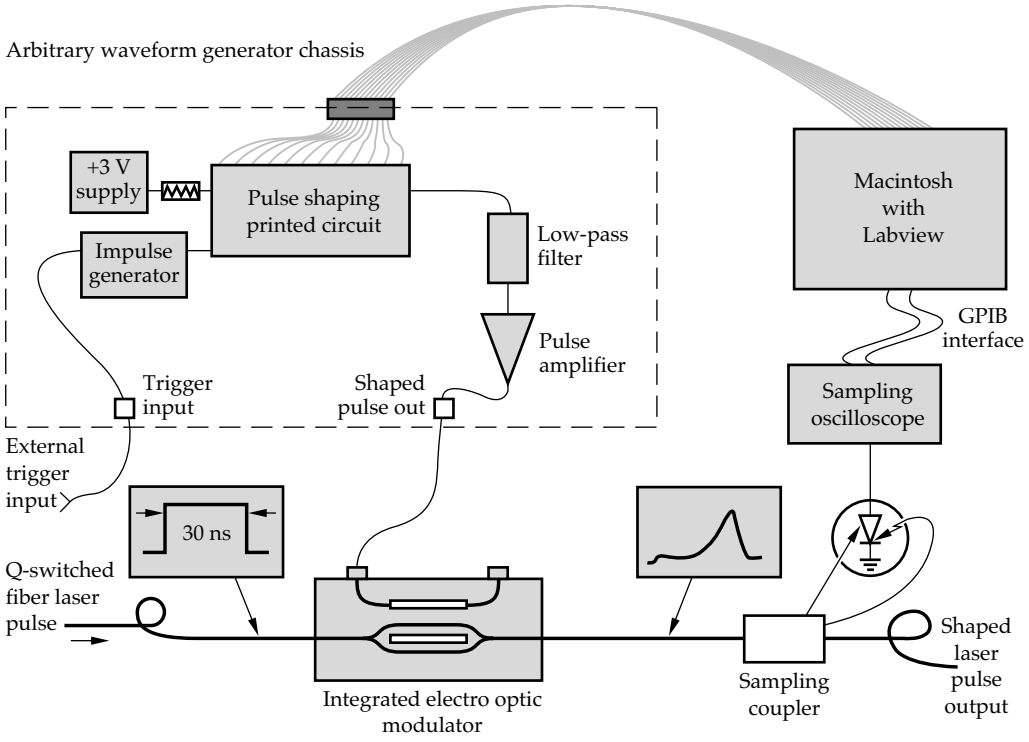

FIGURE 8. Prototype arbitrary optical waveform generation system for the NIF. A 30-ns pulse from the laser oscillator is amplitude-modulated by a Mach–Zehnder electrooptic modulator (only one of the two modulators on the chip is shown). The shape of the optical pulse is measured by a sampling oscilloscope, and the GaAs-FET bias voltages are adjusted until the desired pulse shape is achieved. (70-50-0396-0511pb01)

The AWG circuit is connected to the other supporting electronics. One of the key electronics is the impulse generator that generates the 300-ps trigger pulse. Originally we used an expensive, commercially available generator, but we found that a fixed-width impulse generator consisting of an avalanche diode and a chain of step recovery diodes, originally developed for impulse radar,[13] worked just as well for a small fraction of the price. The impulse generator as designed had a 170-ps FWHM pulse width at 28 V, which we stretched to 300 ps and attenuated to 4 V. The pulse shaping circuit is connected to a control computer that has 32 channels of 12-bit digital-to-analog output for setting the bias on each of the GaAs-FET stages. The shaped electrical pulse, nominally 1 V peak, is low-pass–filtered to remove the 4-GHz sampling noise and is amplified to 5 V to drive an integrated electrooptic modulator. The modulator is an integrated Mach–Zehnder interferometer, similar to that used in the Beamlet front end. The shaped optical pulse is sampled and diagnosed by a fast diode detector and sampling scope, and software written in Labview adjusts the pulse-shaping bias voltages to set and maintain the required optical pulse shape.

Experimental Results

The pulse-shaping system installed on Beamlet has been used to generate a number of relevant pulse shapes that are used (or planned to be used) in Nova, Beamlet, and NIF. Figure 9 shows the generation of a NIF-like pulse: it has the general shape of a NIF-like pulse, but the contrast is reduced to accommodate the diagnostics, and the overall pulse length is shortened to 7 ns to accommodate the subscale waveform generator. Generating this and other pulses is quite simple using feedback software written in Labview, which works in closed loop to minimize the error between the desired pulse and the pulse measured by the diagnostics. Generating a new pulse shape requires only that the user make a (time,intensity) text file, consisting of unequally spaced X-Y pairs in a two-column format. To attain the pulse peak, the feedback control system is not required to fit to the ideal pulse beyond the peak, instead the precipitous drop at the end of the pulse is handled by a pulse slicer. The contrast necessary for NIF has been demonstrated by this system where the electrical pulse was measured directly, instead of the optical pulse being measured. The electrooptic modulator has a $\sin^2(V/V_1)$ response, so for 500:1 optical contrast we need only 25:1 electrical contrast. This is easily measured by the system. However, practical operation with a 500:1 dynamic range demands two transient digitizer channels interfaced to the control system to accurately measure the foot and the peak. This task will be accomplished by mid-1997.

The pulse shape shown in Fig. 10 is the laser pulse required to produce a 3-ns FWHM temporally gaussian laser pulse at the frequency converted (351-nm) wavelength of Beamlet. The temporal shape was calculated by back propagating the tripled light through the frequency converters and the laser chain, back to the AWG. This pulse was useful for benchmarking previous small-spot laser damage experiments[14] against large-aperture Beamlet damage tests.

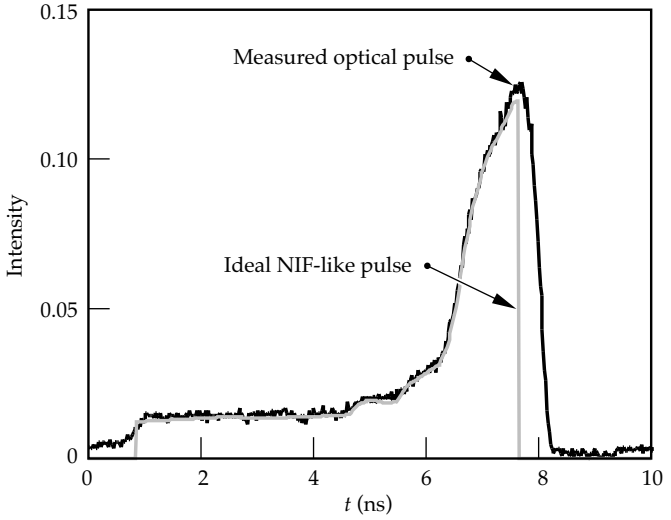

FIGURE 9. NIF-like pulse generated on a 7-ns (28-section) AWG. The NIF pulse is characterized by a long foot followed by a relatively short drive pulse. (70-50-0396-0512pb01)

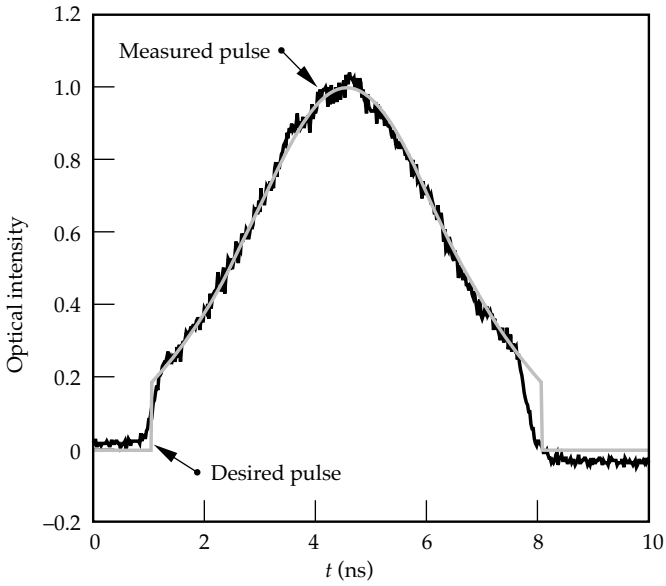

FIGURE 10. Optical pulse used for optics damage experiments. The object of this pulse was to generate a Gaussian-shaped 3-ns-FWHM 3ω pulse from Beamlet. (70-50-0396-0544pb01)

Alternative Applications

In addition to pulse shaping for ICF lasers, precision pulse shaping has several other notable applications that are being pursued. One application is its obvious use as a high-speed modulator of lasers for fiber-optic communications. We have been investigating the possibility of directly connecting the GaAs-FET stages to bit lines of a high-speed computer bus and clocking the data at multigigahertz speeds onto fiber-optic networks. For such a system, the AWG would be operated in the digital mode, in essence as a high-speed multiplexer. The present state of the art is up to 10 GB/s using very expensive GaAs chip-sets. Our AWG technology presents the possibility to operate in excess of 20 GB/s while offering significantly reduced costs relative to the other systems. This system also shows potential for preshaping data communication pulses to compensate for path-pulse distortion in long-haul telecommunications transmission.

Another application currently being pursued is a localized wave-mode generator. Localized wave modes are a form of radar pulses requiring precisely temporally shaped basis modes that, when a reconstructed in the far field, have been shown to stay localized in excess of ten times beyond that predicted by classical diffraction theory. To date, owing to the difficulty in producing subnanosecond shaped electromagnetic pulses, the only demonstration of such modes has been done using acoustic waves in water. Using the AWG to generate electrical pulses, we have already propagated individual 300-MHz localized wave-basis modes from a broadband antenna. The next step is to construct a 5×5 array of such radiators and verify the existence of localized wave modes in free space.

Conclusions

We have developed a computer-controlled arbitrary waveform generator that satisfies the NIF requirements for flexible laser pulse shaping. Technical advancements in a GaAs-FET–based wave summing architecture, element compensation, and efficient trigger-pulse distribution have been very successful in this demonstration. The 7-ns version of the arbitrary waveform generator fielded on the Beamlet laser has produced a number of challenging pulses for Beamlet experiments. Vendor development and production of a full NIF-length generator has begun, with the first prototype due for testing in the first half of fiscal year 1997. The NIF will require 192 such arbitrary waveform generators to be fielded by the year 2000.

Notes and References

1. J. Lindl, *Phys. Plasmas*, **2** (11), 3955–3957 (1995).
2. *National Ignition Facility Conceptual Design Report,* Lawrence Livermore National Laboratory, 7000 East Avenue P. O. Box 808, Livermore, CA 94550, UCRL-PROP-117093 Vol. 3.
3. E. Storm, *Laser Program Annual Report 84*, Lawrence Livermore National Laboratory, Livermore, CA, UCRL-50021-84, p. 2-13.
4. R. B. Wilcox, *Lasers and Particle Beams*, **4**,141–143 (1986).
5. G. M. McWright, *Rev. Sci. Instrum.* **56**(11), 2151–2153 (1985).
6. S. C. Burkhart and R. B. Wilcox, *IEEE Trans. on Microwave Theory Tech*., Vol. 38, pp. 1514–1518, 1990.
7. J. H. Campbell et. al., *ICF Quarterly Report* **5**(1), 1–85, Lawrence Livermore National Laboratory, Livermore, CA, UCRL-LR-105821-95-1 (1995).
8. B. M. Van Wonterghem et. al., *ICF Quarterly Report* **3**(1), 1–9, Lawrence Livermore National Laboratory, Livermore, CA, UCRL-LR-105821-93-1 (1993).
9. M. Haner and W. S. Warren, *Applied Optics*, **26**, 3687–3694 (1987).
10. M. Haner and W. S. Warren, *Appl. Phys. Lett.* **52**, 1458–1460 (1988).
11. S. C. Burkhart, *Voltage-Controlled MESFET Pulse Shape Generator*, LLNL internal report, Lawrence Livermore National Laboratory, Livermore, CA, UCRL-ID-116054 (1994).
12. J. M. Golio, *Microwave MESFETs 1/2 HEMTs*, Norwood, MA, Artech House, 1991, pp. 219–229.
13. T. E. McEwan, R. L. Hanks, and J. D. Kilkenny, *High-Voltage Picosecond Pulse Generation Using Avalanche Diodes*, LLNL internal report, Lawrence Livermore National Laboratory, Livermore, CA, UCRL-102565 (1990).
14. L. Sheehan et. al., *Proc. 25th Annual Boulder Damage Symposium*, **2114**, 559–568, SPIE, Bellingham, Washington (1993).